International Journal of Nanomedicine

Dovepress
open access to scientific and medical research

Open Access Full Text Article

ORIGINAL RESEARCH

Enhancement of Radiosensitization by Silver Nanoparticles Functionalized with Polyethylene Glycol and Aptamer As1411 for Glioma Irradiation Therapy

This article was published in the following Dove Press journal:
International Journal of Nanomedicine

Jing Zhao[1]
Peidang Liu[1,2]
Jun Ma[3]
Dongdong Li[1]
Huiquan Yang[1]
Wenbin Chen[1]
Yaowen Jiang[2]

[1]School of Medicine, Southeast University, Nanjing 210009, People's Republic of China; [2]Jiangsu Key Laboratory for Biomaterials and Devices, Southeast University, Nanjing 210096, People's Republic of China; [3]Radiotherapy Department, Affiliated Hospital of Nanjing University of Chinese Medicine, Nanjing 210029, People's Republic of China

Background: The efficacy of radiotherapy for glioma is often limited by the radioresistance of glioma cells. The radiosensitizing effects of silver nanoparticles (AgNPs) on glioma were found in the previous studies of our group. In order to enhance the radiosensitivity of tumor cells and selectively kill them while reducing the side effects of irradiation therapy, targeted modification of AgNPs is urgently needed.

Materials and methods: In the present study, AgNPs functionalized with polyethylene glycol (PEG) and aptamer As1411 (AsNPs) were synthesized and subsequently characterized by transmission electron microscopy, ultraviolet-visible spectroscopy and Fourier transform infrared spectroscopy. Then the targeting property of AsNPs was evaluated by dark-field imaging, confocal microscopy and in vivo imaging. Both colony formation assay and glioma-bearing mouse model were employed to study the radiosensitizing effect of AsNPs.

Results: The characterization results revealed a spherical shape of AgNPs with an average diameter of 18 nm and the successful construction of AsNPs. AsNPs were confirmed to specifically target C6 glioma cells, but not normal human microvascular endothelial cells. Moreover, AsNPs could not only internalize into tumor cells, but also penetrate into the core of tumor spheroids. In vitro experiments showed that AsNPs exhibited a better radiosensitizing effect than AgNPs and PEGylated AgNPs (PNPs), inducing a higher rate of apoptotic cell death. In vivo imaging demonstrated that Cy5-AsNPs preferentially accumulated at the tumor site, and the ratio of fluorescence intensity of Cy5-AsNPs to that of Cy5-PNPs reached the maximum at 6 h post-systemic administration. Furthermore, the combination of AsNPs with irradiation significantly prolonged the median survival time of C6 glioma-bearing mice.

Conclusion: Our results indicated that AsNPs could be an effective nano-radiosensitizer for glioma targeting treatment.

Keywords: radiosensitization, As1411, silver nanoparticles, glioma

Introduction

Malignant gliomas are common and aggressive primary cerebral tumors with significant mortality.[1,2] Current treatment options for diagnosed patients are multimodal, including surgical resection, radiotherapy and chemotherapy. However, the heterogeneous and highly infiltrative nature of malignant glioma makes complete surgical resection almost impossible.[3] Radiotherapy is a standard adjuvant treatment and shows a survival benefit for glioma patients, but its therapeutic efficacy is

Correspondence: Peidang Liu
School of Medicine, Southeast University, 87 Dingjiaqiao Road, Nanjing 210009, Jiangsu Province, People's Republic of China
Tel/Fax +86 25 8327 2554
Email seulpd@163.com

submit your manuscript | www.dovepress.com
DovePress
http://doi.org/10.2147/IJN.S224160

often limited due to the radioresistance of glioma cells.[4,5] Furthermore, the conventional radiotherapy is poorly selective for tumor cells that usually induces a series of radioactive damages to the surrounding normal tissues.[6] Therefore, it is still a challenge to enhance radiosensitivity of glioma cells and reduce the side effects of irradiation.

With the remarkable advancements of nanotechnology, several types of metal or metal oxide nanomaterials have been developed to enhance the anticancer efficacy of radiotherapy. Among these nanomaterials, silver nanoparticles (AgNPs) and gold nanoparticles have attracted particular attention owing to their excellent radiosensitizing properties.[7–10] Our previous studies confirmed the radiosensitizing potential of AgNPs on glioma cells in vitro and in vivo, which was much more efficient than that of gold nanoparticles at the same molar and mass concentrations.[7,11–13] However, the application of AgNPs in radiotherapy is restricted because of the following limitations: 1) the unmodified AgNPs have poor selectivity for tumor cells, which triggers some side effects; and 2) the stereotactic administration of AgNPs inevitably causes physical damage to the brain and heterogeneous distribution of the nanoparticles in tumors. To address these issues, we have been attempting to develop modified AgNPs for targeting glioma via systemic administration.

Ligand-mediated active targeting plays a crucial role in the targeted delivery system. Owing to the immunogenicity and competitive nature of endogenous ligands,[14] exogenous ligands, such as aptamers and peptides, have emerged as attractive novel targeting agents.[15,16] Aptamers are synthesized single-strand DNA or RNA oligonucleotides by an in vitro selection and amplification method called SELEX, and are designed to identify the specific molecular targets, such as nucleic acids and proteins, and even cells with high specificity and selectivity. As1411 is a G-rich DNA aptamer that can be exploited for cancer diagnosis and treatment. It exhibits high binding affinity to nucleolin, a protein overexpressed on the plasma membrane of cancer cells but not on that of normal cells.[17,18]

The aim of the present study was to construct AgNPs functionalized with polyethylene glycol (PEG) and As1411 (AsNPs), and assess their tumor-targeting property and radiosensitizing effect both in vitro and in vivo. Our results will provide an important basis for the potential application of AsNPs as an effective nano-radiosensitizer for the targeted treatment of glioma.

Materials and Methods

Materials

As1411 (sequence: 5′-GGTGGTGGTGGTTGTGGTGGTG GTGG-3′, 5′-$(CH_2)_6$-NH_2) was synthesized by Sangon Biotech Co., Ltd. (Shanghai, China). Dulbecco's modified Eagle's medium (DMEM) and fetal bovine serum (FBS) were ordered from Gibco (Carlsbad, CA, USA). Polyvinylpyrrolidone (PVP, K30), 3-[4,5-dimethylthiazol-2-yl]-2,5-diphenyltetrazolium bromide (MTT), Annexin V-FITC/PI Apoptosis Detection Kit, 4′,6-diamidino-2-phenylindole dihydrochloride (DAPI), 1,1′-dioctadecyl-3,3,3′,3′-tetramethylindodicarbocyanine (DiD), fluorescein isothiocyanate (FITC), dimethyl sulfoxide (DMSO), *N*-hydroxysuccinimide (NHS) and *N*-(3-dimethylaminopropyl)-*N*′-ethyl carbodiimide hydrochloride (EDC) were purchased from Sigma-Aldrich (St. Louis, MO, USA). Thiol-terminated monomethoxy polyethylene glycol (HS-PEG-OMe, MW = 2000 Da) and thiol-terminated carboxyl polyethylene glycol (HS-PEG-COOH, MW = 2000 Da) were custom synthesized by JenKem Technology Company (Beijing, China). C6 glioma cell line was obtained from the Type Culture Collection of the Chinese Academy of Sciences (Shanghai, China). Human microvascular endothelial cells (HMEC-1) were purchased from the American Type Culture Collection (Manassas, VA, USA). BALB/c nude mice (female, 16–18 g) were obtained from the Comparative Medicine Center of Yangzhou University (Yangzhou, China) and maintained under standard housing conditions. The Ethics Committee of Southeast University approved the experiments, and the animals were cared for according to the protocols evaluated and approved by the committee.

Synthesis of AsNPs

The PVP coated AgNPs were prepared by electrochemical synthesis method which has been reported previously.[19] Firstly, two silver rods were polished and installed on the cover of the electrolytic reactor. Then, PVP solution (5 mg/mL) was pumped into the electrolytic reactor continuously at the flow velocity of 60 mL/h, meanwhile a voltage of 10 V was applied to the silver electrodes. The reaction temperature was 60°C and the polarity of the anode and cathode was exchanged every minute. Finally, the AgNPs solution was collected by centrifugation at 18,000 rpm for 40 min and stored at 4°C.

For the As1411 conjugation, HS-PEG-COOH and HS-PEG-OMe were mixed in a molar proportion of 1:19 and reacted with AgNPs for 12 h in the dark. The HS-PEG was

conjugated to the surface of AgNPs and the PEGylated AgNPs (PNPs) were obtained. Subsequently, the carboxyl units of PNPs were activated using EDC and NHS in pH 6.0 2-(*N*-morpholino)ethanesulfonic acid (MES) buffer for 4 h. The MES buffer was then replaced by phosphate-buffered saline (PBS, pH 7.4), As1411 was added into the PNPs suspension and the resulting mixture was stirred for 24 h in the dark. Next, the mixture was transferred to dialysis bags (MWCO: 20 kDa) and dialyzed for 48 h to remove the residual PEG and As1411. Eventually, AsNPs solution was collected by centrifugation and stored at 4°C for further experiments.

Characterization of AsNPs

The morphology and size of AgNPs were observed by transmission electron microscopy (TEM; JEM-2000EX, Hitachi, Tokyo, Japan), and the mean size was determined by counting over 200 particles in representative TEM images. The hydrodynamic sizes and zeta potentials of AgNPs, PNPs and AsNPs were measured by dynamic light scattering (DLS; Nano ZS, Malvern Instruments, Malvern, UK). The successful construction of AsNPs was verified by ultraviolet-visible (UV-vis) spectroscopy (UV-3600, Shimadzu, Japan) and Fourier transform infrared (FTIR) spectroscopy (Nicolet iS50, Thermo Scientific, MA, USA). The final concentration of silver in aqueous solution was measured by inductively coupled plasma mass spectrometry (ICP-MS; 7500a, Agilent, CA, USA).

Cell Culture and Proliferation Assay

C6 cells were cultured in DMEM medium supplemented with 10% FBS and penicillin-streptomycin (100 U/mL) in a 5% CO_2 humidified chamber at 37°C.

The nanoparticle-induced cytotoxicity was analyzed by MTT assay. Briefly, C6 cells (10^3 cells/100 μL) were seeded in 96-well plates and cultured for 24 h. After exposure to AgNPs, PNPs or AsNPs with different concentrations (0, 15, 30, 60, 120 and 240 μg/mL) for 24 h, the cells were washed three times with PBS to remove the extra nanoparticles. After that, the medium was replaced by a mixture of DMEM medium (80 μL) and MTT (20 μL, 5 mg/mL), and the cells were incubated for a further 4 h. The DMEM/MTT mixture was then removed and 150 μL DMSO was added to each well to fully dissolve the formed formazan crystals. Finally, the absorbance of each well at 570 nm was measured using a Multiskan FC microplate photometer (Thermo Scientific, MA, USA). The experiments were performed in triplicate, and the half maximal inhibitory concentration (IC_{50}) was calculated using GraphPad Prism software (version 8.0, GraphPad Software, Inc., USA).

Cellular Uptake of AsNPs

C6 cells were seeded in 24-well plates with round coverslips at the density of 2×10^4 cells per well. The next day, C6 cells were incubated with medium containing 30 μg/mL AgNPs, PNPs or AsNPs for different time periods (0.5, 1.5, 3, 6, 12, 24 or 48 h). After incubation, the cells were washed three times with PBS and fixed with 4% paraformaldehyde. Finally, the cells were observed using a dark-field microscope (Eclipse E200, Nikon, Tokyo, Japan).

Evaluation the Targeting Property of AsNPs in vitro

Since nucleolin is a protein overexpressed on the plasma membrane of tumor cells but not on that of normal cells, it was expected that the AsNPs could be specifically recognized by tumor cells. The selectivity of AsNPs for C6 tumor cells over normal HMEC-1 cells was confirmed by dark-field microscopy and confocal laser scanning microscopy. C6 and HMEC-1 cells (2×10^4 per well) were seeded and cultured overnight in 24-well plates with round coverslips. Then the cells were incubated with or without 30 μg/mL AsNPs for 12 h and directly visualized by dark-field microscopy after washing three times with PBS. While the cells, stained with DiD fluorescent dye for 20 min and then counterstained with 0.5 mg/mL DAPI for 5 min, were examined by confocal laser scanning microscopy (CLSM; FluoView FV1000, Olympus, Hamburg, Germany) to determine the intracellular localization of AsNPs.

Evaluation of Tumor Spheroid Penetration

A C6 glioma spheroid model was established as previously.[20] In brief, C6 cells (2×10^3 per well) were seeded in 48-well plates coated with 2% low-melting-temperature agarose (150 μL). Three-dimensional tumor spheroids were obtained after seven days of growth and treated with or without 50 μg/mL FITC-loaded PNPs or FITC-loaded AsNPs. After 6 h or 12 h of incubation, the tumor spheroids were rinsed three times with PBS and fixed with 4% paraformaldehyde for 15 min. At last, the spheroids were transferred to glass slides and covered with an anti-fluorescence quenching agent. The fluorescence intensity was observed by CLSM using an excitation wavelength of 488 nm.

Irradiation Treatment

For the irradiation groups, C6 cells were washed three times with PBS after exposure to nanoparticles for 24 h and irradiated with 6 megavolt (MV) X-rays at a dose rate of 200 cGy/min. At the same time, control cells were removed from the incubator without irradiation exposure.

Clonogenic Survival Assay

The antiproliferative efficacy of the combination of AsNPs and irradiation was evaluated by colony formation assay. C6 cells were seeded in 6-well plates at a density of 10^4 cells per well and incubated overnight. Then cells were divided into the following groups: control, AgNPs, PNPs, AsNPs and their corresponding irradiation treatment groups. AgNPs, PNPs or AsNPs were mixed with cell culture medium and added to each well at the same concentration (30 μg/mL). After 12 h, the solution was replaced with fresh culture medium. Irradiation groups were irradiated at the doses of 2, 4, 6 and 8 Gy, respectively. After that, C6 cells were trypsinized, counted and seeded (500 cells) in 6-well plates. Following incubation for 7 days, C6 cells were fixed and stained with Giemsa staining, and the colonies containing more than 50 cells were counted. The cell survival curve was fitted according to the multitarget single-hit model and the sensitization enhancement ratio (SER) was calculated.

Cell Apoptosis

The apoptosis-inducing capabilities of AgNPs, PNPs or AsNPs with or without irradiation were assessed by Annexin V-FITC/PI apoptosis detection assay. Briefly, following the treatment as described earlier, irradiation groups received a single dose of 6 Gy X-ray irradiation. Twenty-four hours later, C6 cells were collected and washed three times with PBS, and then resuspended in 200 μL binding buffer at the concentration of 10^6 cells/mL. Next, 5 μL Annexin V-FITC and 10 μL PI were consecutively added into the above binding buffer, and the cells were incubated for 20 min at room temperature. Finally, samples were immediately measured using flow cytometry (NovoCyte, ACEA, CA, USA).

In vivo Imaging

To investigate the distribution of AsNPs in vivo, Cy5-labeled PNPs and Cy5-labeled AsNPs were prepared and injected into the glioma-bearing mice via the tail vein, respectively. BALB/c nude mice were anesthetized with 0.4% sodium pentobarbital and individually placed in a stereotaxic apparatus (RWD Life Science, Shenzhen, China). C6 cells (10^6 cells in 5 μL PBS) were injected into the right striatum (2 mm lateral and 0.5 mm anterior to the bregma, 3 mm depth from the dura) at a rate of 1 μL/min. After that, the needle was left in place for 5 min and then slowly withdrawn. The skin closure of surgical incision was closed with sutures, and the animals were returned to animal room. Nine days after tumor cells implantation, the mice were intravenously administered Cy5-labeled PNPs or Cy5-labeled AsNPs at a dose of 10 mg/kg. The glioma-bearing mice were anesthetized with isoflurane and imaged under an in vivo imaging system (Night OWL II LB983, Berthold Technologies, Bad Wildbad, Germany) at predetermined time intervals. Forty-eight hours after administration of the nanoparticles, the mice were sacrificed and the brain fluorescence intensity was detected. The fluorescence intensity ratio of Cy5-labeled AsNPs to PNPs at tumor site was calculated.

In vivo Antiglioma Effect of AsNPs Plus Irradiation

The nude mice bearing brain glioma were obtained as described above. Nine days after tumor implantation, the mice were randomly divided into eight groups and systemically administered 150 μL saline or nanomaterial solution at a dose of 10 mg/kg (eight mice per group): saline, AgNPs, PNPs, AsNPs, irradiation, AgNPs + irradiation, PNPs + irradiation, and AsNPs + irradiation. Six hours after injection, the mice in irradiation groups were anesthetized and irradiated by 6 MV X-ray beams (6 Gy per mouse). After the treatment, the animals were observed daily for any changes in clinical appearance and the times of death were recorded to calculate the median survival time (MST).

Statistical Analysis

All obtained data were presented as the mean ± standard deviation (SD). The paired Student's *t*-test was used for statistical analysis of clonogenic assay. The survival analysis was done using the Kaplan-Meier survival curve and the log rank test. Remaining data were analyzed by one-way ANOVA test. A P value of less than 0.05 was considered significantly different.

Results and Discussion

Preparation and Characterization of AsNPs

The preparation process of AsNPs includes three major steps, as illustrated in Figure 1A. In the first step, the PVP coated AgNPs were synthesized. Subsequently, HS-PEG was conjugated with AgNPs through silver-thiol interaction and the

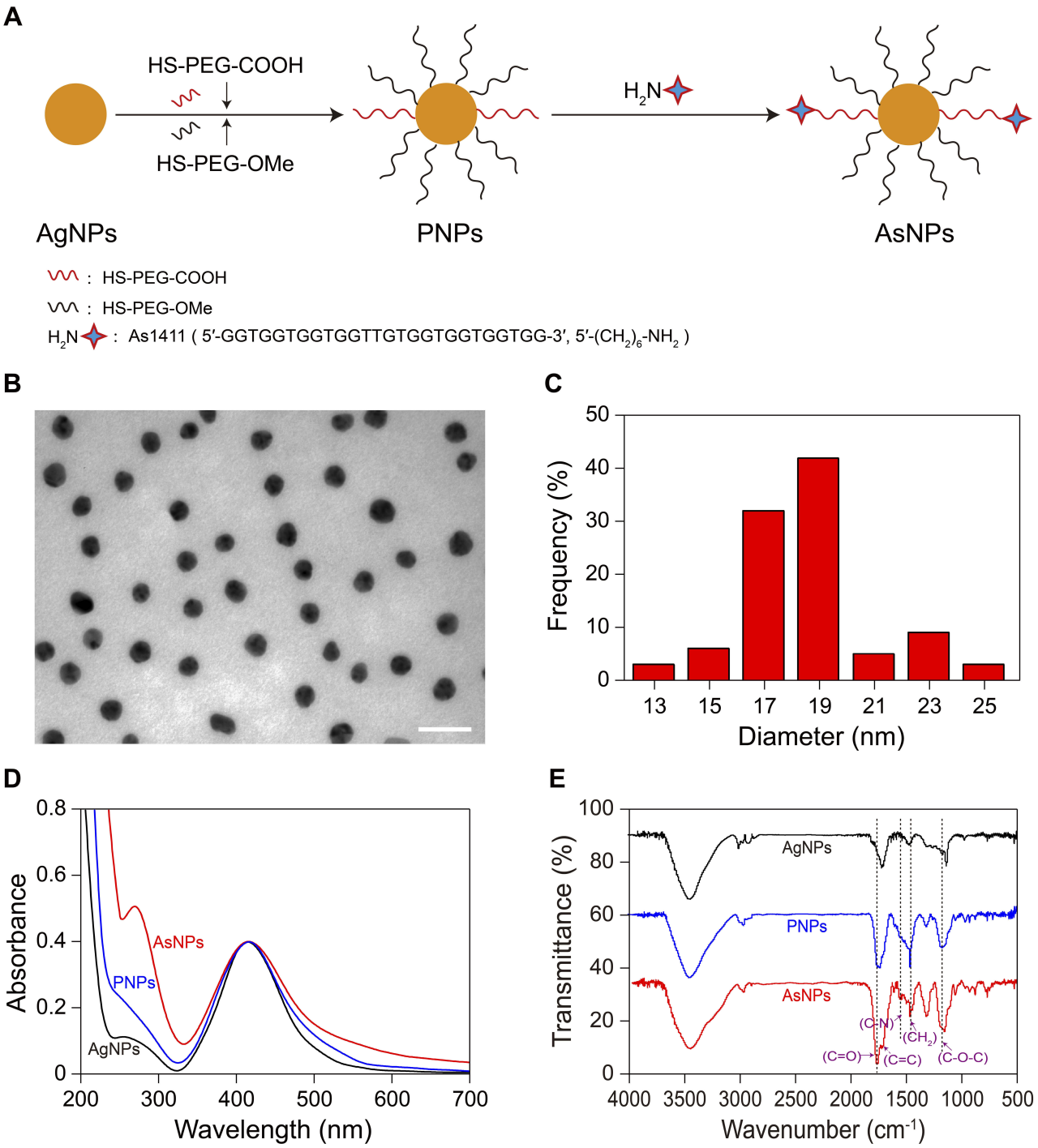

Figure 1 Characterization of AgNPs, PNPs and AsNPs.

Notes: (**A**) Schematic diagram depicting the synthesis of AsNPs. (**B**) The typical TEM image and (**C**) corresponding size distribution histogram of AgNPs. The size distribution histogram was obtained by size analysis of over 200 particles. The mean diameter was 18 ± 2 nm. Scale bar: 50 nm. (**D**) UV-vis spectra and (**E**) FTIR spectra of AgNPs, PNPs and AsNPs.

Abbreviations: AgNPs, silver nanoparticles; PNPs, PEGylated silver nanoparticles; AsNPs, PEG- and As1411-functionalized silver nanoparticles; TEM, transmission electron microscopy; nm, nanometer; UV-vis, ultraviolet-visible; FTIR, Fourier transform infrared spectroscopy.

PNPs were obtained. Finally, As1411 was conjugated to the surface of PNPs via the reaction of amino and carboxyl and the AsNPs were constructed. TEM images showed that AgNPs were generally spherical and well dispersed, with an average diameter of 18.82 ± 2.10 nm (Figure 1B and C). The UV-vis spectra of AgNPs, PNPs and AsNPs all exhibited a strong surface plasmon absorption peak at approximately 408 nm (Figure 1D), which is in accordance with the characteristic absorption band of AgNPs. After functionalization with PEG and As1411, a slight red shift (from 408 to 414 nm)

of the surface plasmon band was observed, and the characteristic absorption peak of the aptamer emerged at about 260 nm, indicating the successful construction of AsNPs. The FTIR spectrum of AsNPs contained strong absorption peaks at 2851, 1375 and 1100 cm^{-1} (Figure 1E), corresponding to the CH_2 stretching, CH_2 bending and C–O–C stretching vibrations in PEG molecules, which was right in line with previous studies.[21] In addition, two bands were observed at 1649 and 1411 cm^{-1}, corresponding to the C=C stretching and C-N bending vibrations of the amide bonds in the As1411 moiety. The FTIR results further confirmed the conjugation of PEG and As1411 on the surfaces of AgNPs.

DLS is a useful technique to evaluate the size and other characteristics of nanomaterials in solution.[22] The results of hydrodynamic diameters and zeta potentials of AgNPs, PNPs and AsNPs in distilled water are shown in Table 1. The hydrodynamic diameter of AgNPs was larger than the average diameter obtained from the TEM images due to the thickness of the hydration shell. Then it significantly decreased following conjugation with PEG, because PEG could increase the water solubility of nanoparticles.[23] Besides, the negative charge of As1411 lowered the zeta potential of AsNPs and made them much more stable owing to the increased electrostatic repulsion.

Cytotoxicity of AsNPs

For biomedical application of nanoparticles, it is essential to evaluate their cytotoxic potential.[24] The cytotoxic effects induced by different surface modified AgNPs on C6 cells were evaluated by MTT assay. The AgNPs, PNPs and AsNPs with different concentrations ranging from 15 to 240 μg/mL exhibited increased cytotoxicity in a dose-dependent manner after incubation for 24 h (Figure 2), but they had little effect on the viability of normal cells (Figure S1). The antiproliferative IC_{50} values of AgNPs, PNPs and AsNPs in C6 glioma cell line were 300, 569 and 462 μg/mL, respectively. In the subsequent experiments involving cells, a concentration of 30 μg/mL (1/10 IC_{50} value of AgNPs) was used, because at this concentration the nanoparticles possessed potential radiosensitizing activity without significant cytotoxicity.

Due to their diversified surface modifications, nanoparticles exert distinct physicochemical properties and cytotoxicities.[25] In the efforts to develop safe and efficient nanomaterials, PEG, a nonionic hydrophilic polymer, has been widely used because of its excellent characteristics. For instance, PEG can greatly improve the water solubility and decrease the cytotoxicity of nanoparticles.[26] Moreover, the reactive groups of PEG are beneficial to the modification of nanomaterials.[27] In the present study, PEGylated AgNPs demonstrated lower cytotoxicity than PVP coated AgNPs.

Table 1 Hydrodynamic Sizes, Polydispersity Indexes and Zeta Potentials of AgNPs, PNPs and AsNPs

Sample	Hydrodynamic Size (nm)	Polydispersity Index	Zeta Potential (mV)
AgNPs	69.08 ± 0.57	0.255	−14.19 ± 1.04
PNPs	33.31 ± 0.92	0.232	−16.06 ± 2.04
AsNPs	37.80 ± 3.13	0.244	−21.30 ± 4.99

Abbreviations: AgNPs, silver nanoparticles; PNPs, PEGylated silver nanoparticles; AsNPs, PEG- and As1411-functionalized silver nanoparticles; nm, nanometer; mV, millivolt.

In vitro Cellular Uptake and Tumor Spheroid Penetration of AsNPs

The amount of internalized nanoparticles is essential for inducing damage to tumor cells.[28] In the current study, dark-field imaging was employed to evaluate the cellular uptake of AgNPs, PNPs and AsNPs by C6 glioma cells. Only weak outlines of the cells in the dark background could be observed in control group, whereas bright spots corresponding to the

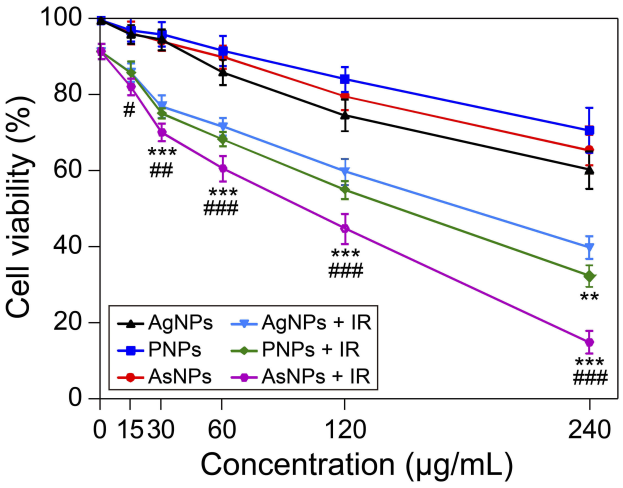

Figure 2 Effects of AgNPs, PNPs and AsNPs on C6 cell viability with or without irradiation.

Notes: C6 cells were incubated with different concentrations of AgNPs, PNPs or AsNPs for 24 h. Twenty-four hours after 4 Gy X-ray irradiation treatment, cell viability was evaluated by MTT assay. Data are shown as the mean ± SD (n = 3). IR in the figure is an abbreviation for irradiation. $^{**}P<0.01$, $^{***}P<0.001$ compared with the corresponding AgNPs treated group; $^{\#}P<0.05$, $^{\#\#}P<0.01$, $^{\#\#\#}P<0.001$ compared with the corresponding PNPs treated group.

Abbreviations: AgNPs, silver nanoparticles; PNPs, PEGylated silver nanoparticles; AsNPs, PEG- and As1411-functionalized silver nanoparticles; h, hours; Gy, gray; MTT, 3-[4,5-dimethylthiazol-2-yl]-2,5-diphenyltetrazolium bromide; SD, standard deviation; n, number.

nanoparticles were clearly visualized in the nanoparticles treated groups (Figure 3A). A certain amount of AgNPs was found in C6 cells even though the incubation time was prolonged to 48 h. However, the amount of intracellular PNPs was significantly increased and reached the peak level at 12 h incubation time, and then it slightly decreased with time. The time to reach the peak level was the same in AsNPs treated group, but the amount of internalized nanoparticles was much higher and maintained at the peak level up to 48 h compared with that of PNPs treated group. ICP-MS was also performed to quantitatively analyse the amount of internalized nanoparticles, and the results were consistent with that of dark-field

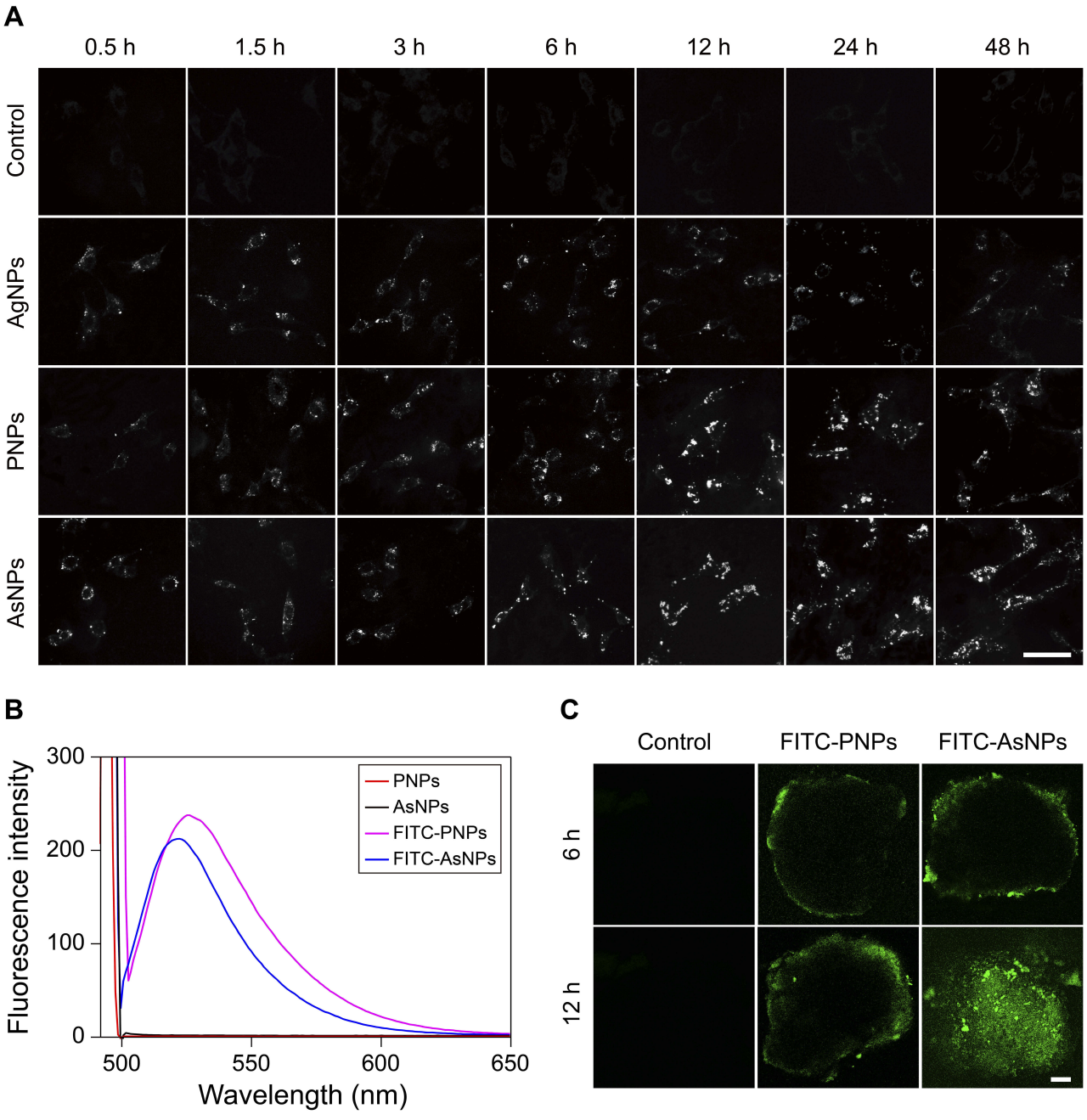

Figure 3 Cellular uptake and tumor spheroid penetration of AsNPs.

Notes: (**A**) Cellular uptake of AgNPs, PNPs and AsNPs as assessed by dark-field imaging. The bright spots represented the nanoparticles, and the amount of intracellular AsNPs significantly increased with incubation time and reached the peak at 12 h incubation time. Scale bar: 25 μm. (**B**) The fluorescence spectra of FITC-PNPs and FITC-AsNPs. (**C**) The tumor penetration of FITC-PNPs or FITC-AsNPs in a C6 glioma spheroid model. In confocal images, green fluorescence signals indicated FITC-PNPs or FITC-AsNPs. FITC-AsNPs could penetrate into the core of the spheroid at 12 h incubation time while FITC-PNPs were only distributed at the growing edge of tumor spheroid. Scale bar: 100 μm.

Abbreviations: AsNPs, PEG- and As1411-functionalized silver nanoparticles; AgNPs, silver nanoparticles; PNPs, PEGylated silver nanoparticles; h, hours; μm, micrometer; FITC-PNPs, fluorescein isothiocyanate-loaded PEGylated silver nanoparticles; FITC-AsNPs, fluorescein isothiocyanate-loaded PEG- and As1411-functionalized silver nanoparticles.

imaging (Figure S2). These data indicated that the surface modifications with PEG and As1411 could effectively enhance the endocytosis of AgNPs into tumor cells.

Effective penetration of nanoparticles into solid tumors is a major challenge in cancer therapy.[29,30] Three-dimensional tumor spheroid could mimic the in vivo status of solid tumors.[31] Thus, we studied the tumor penetration of AsNPs in a C6 glioma spheroid model using CLSM. The fluorescence spectrophotometry results demonstrated that the fluorescence spectra of FITC-PNPs and FITC-AsNPs were in consistent with the excitation wavelength of FITC (Figure 3B), indicating the successful conjugation of FITC on the surfaces of PNPs and AsNPs. The CLSM results showed that the longer incubation times could facilitate the penetration of these nanoparticles. It is worthy to note that, AsNPs could be internalized into the core of spheroid while PNPs only distributed at the growing edge of tumor spheroid (Figure 3C), suggesting that As1411 effectively increased the tumor penetration of the nanoparticles.

Tumor-Targeting Property of AsNPs

In order to evaluate the tumor-targeting property of AsNPs, both in vitro and in vivo experiments were performed in this study. At the cellular level, two methods were utilized to assess the targeting ability of AsNPs to glioma cells. The dark-field images showed that the amount of internalized AsNPs in C6 tumor cells was significantly higher than that in normal HMEC-1 cells (Figure 4A), which was further verified by ICP-MS (Figure S3). In the latter ones, AsNPs were mainly localized around the plasma membrane and rarely appeared in the cytoplasm. Subsequently, CLSM was performed to observe the exact location of AsNPs within the cells. It could be seen that AsNPs were predominantly localized in the cytoplasm of C6 glioma cells, but in non-malignant HMEC-1 cells, they were mostly distributed outside of the cell or located in the plasma membrane (Figure 4B). The difference in AsNPs uptake between C6 glioma cells and HMEC-1 cells is related to the amount of cell surface nucleolin. As a multi-domain protein, nucleolin is continuously expressed on the surface of tumor cells but not on that of normal cells. Its arginine-glycine-glycine domain specifically binds to the G-quadruplex of As1411 and thereby mediates the internalization of As1411 modified nanoparticles in a calcium-dependent manner.[32–34] Taken together, the results presented above indicated that the AsNPs were efficiently and selectively internalized by C6 tumor cells but not by nonmalignant cells. The specific

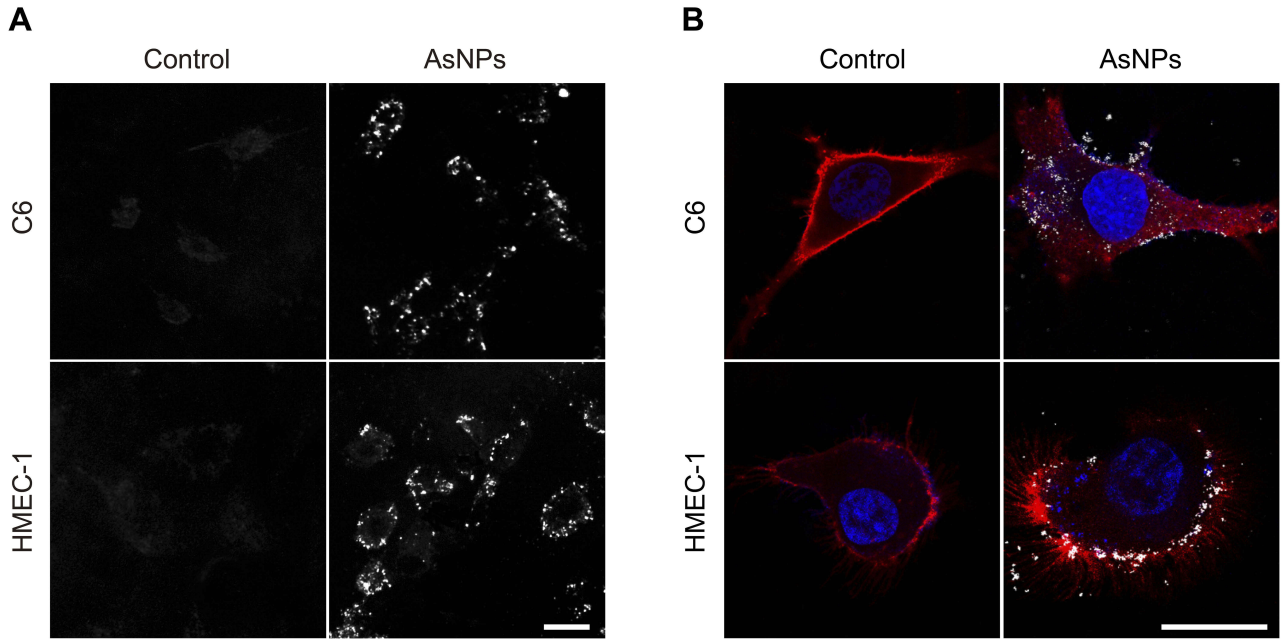

Figure 4 Tumor-targeting property of AsNPs at the cellular level.

Notes: C6 glioma cells and normal human microvascular endothelial cells (HMEC-1) were used in the experiment. (**A**) Representative dark-field images. Scale bar: 25 μm. (**B**) Representative confocal images. The cell membranes were stained with DiD (red color), while the cell nuclei were stained with DAPI (blue color). The bright spots represented AsNPs. Scale bar: 25 μm.

Abbreviations: AsNPs, PEG- and As1411-functionalized silver nanoparticles; μm, micrometer; DiD, 1,1′-dioctadecyl-3,3,3′,3′-tetramethylindodicarbocyanine; DAPI, 4′,6-diamidino-2-phenylindole dihydrochloride.

targeting ability of radiosensitizing agents is beneficial for recognizing the targeted tumor cells while minimizing the dose of radiotherapy and side effects on normal cells.[35]

The in vivo tumor-targeting property of AsNPs was examined via in vivo imaging. Cy5-PNPs or Cy5-AsNPs were systemically administered to nude mice bearing intracranial glioma, and then these mice were imaged at different time intervals. The results showed that Cy5-PNPs spread throughout the whole body along with the blood circulation and were quickly cleared out from the body. The fluorescence signal of Cy5-PNPs in the tumor region was weakened gradually with time. However, the change pattern of fluorescence signal of Cy5-AsNPs in the tumor area was different from that of Cy5-PNPs. The ratio of fluorescence intensity of Cy5-AsNPs to that of Cy5-PNPs reached the maximum at 6 h post-injection (approximately 2.2) (Figure 5A and C). Furthermore, the ex vivo imaging of their brains showed strong accumulation of Cy5-AsNPs at the tumor site, while Cy5-PNPs were completely cleared out from the brain (Figure 5B). These results

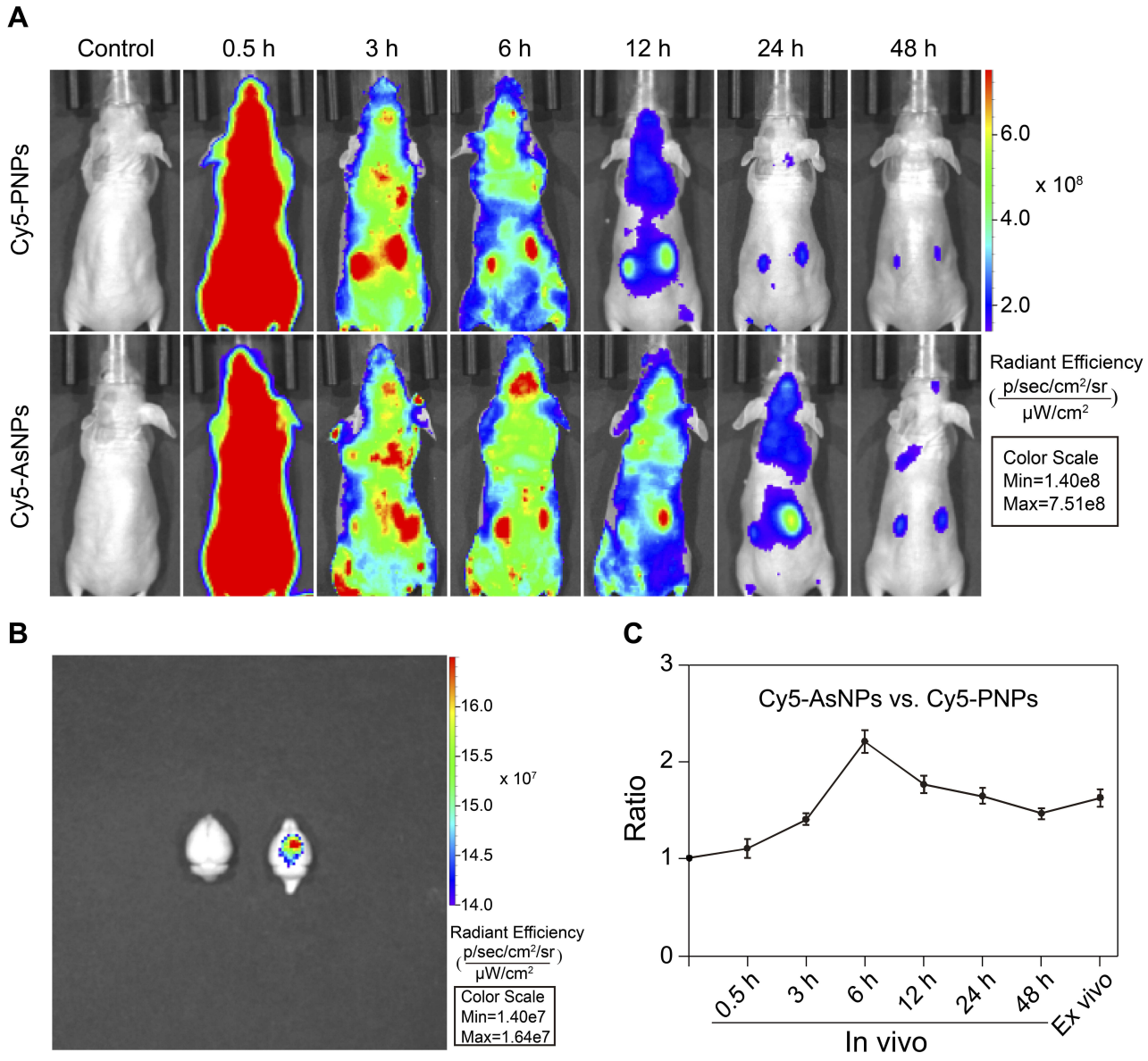

Figure 5 In vivo distribution of AsNPs.

Notes: (**A**) In vivo images of glioma-bearing nude mice. The mice were injected with Cy5-PNPs or Cy5-AsNPs via the tail vein and imaged at different time intervals. (**B**) Ex vivo images of the brains. The mice were perfused at 48 h post-injection, and then ex vivo imaging of the brains was performed. (**C**) The fluorescence intensity ratio of Cy5-AsNPs to that of Cy5-PNPs at the tumor site. Data are shown as the mean ± SD (n = 3).

Abbreviations: AsNPs, PEG- and As1411-functionalized silver nanoparticles; PNPs, PEGylated silver nanoparticles; h, hours; SD, standard deviation; n, number.

indicate that the in vivo tumor-targeting ability of the AgNPs functionalized with PEG and As1411 was superior to that of the AgNPs modified only with PEG.

PEGylated nanoparticles can reduce the interaction with serum proteins and increase circulation time in blood, which allow them to passively accumulate within the tumor interstitium via the enhanced permeability and retention (EPR) effect.[36,37] Moreover, active targeting facilitates the selective uptake of nanoparticles by the tumor cells.[38] Although the relative contribution of EPR effect and active targeting to the targeting efficiency of nanosized materials to the tumor tissues has not been clearly clarified,[39] our study showed it varied with time. Benefiting from both the EPR effect and active targeting, AsNPs could selectively and effectively accumulate at the tumor site.

Radiosensitizing Effect of AsNPs

The radiosensitizing efficacies of AgNPs, PNPs and AsNPs on glioma were observed and compared at both cellular and animal levels. Colony formation assay can reflect the long-term proliferative potential of cancer cells following radiotherapy and is therefore considered to be the gold standard for measuring cellular radiosensitivity in vitro.[40] The radiosensitizing effects of AgNPs, PNPs and AsNPs on C6 glioma cells were evaluated by this method and the results are presented in Figure 6. The surviving fractions decreased rapidly with increasing doses of X-rays, and there was a significant difference between the curves, indicating that all three kinds of materials have abilities to enhance the irradiation effect in glioma cells. The corresponding SER values were 1.22, 1.31 and 1.62, respectively, suggesting that the rank of radiosensitizing abilities from high to low is AsNPs, PNPs, AgNPs. These findings were again proved by the short-term (MTT) assay (Figure 2). The better radiosensitizing activity of AsNPs may be due to their higher intracellular accumulation, since the radiosensitization effects are directly related to the amount of intracellular radiosensitizers.[41,42]

In the in vivo radiosensitization experiment, radiotherapy was performed at 6 h after systemic administration of AgNPs, PNPs or AsNPs, and the survival times of the glioma-bearing mice were obtained and analyzed. The Kaplan-Meier survival curves are presented in Figure 7. The MSTs of the mice treated with saline, AgNPs, PNPs or AsNPs alone were 18, 19, 20 and 22 days, respectively. There was no significant difference among these four groups in terms of MSTs, indicating that both the targeted AgNPs and non-targeted AgNPs had no obvious antitumor effect at this concentration. However, the mice treated with saline, AgNPs, PNPs or AsNPs plus irradiation therapy exhibited a significant increase in MSTs to 24, 30, 35 and 45 days, respectively. The MSTs were statistically different between PNPs plus

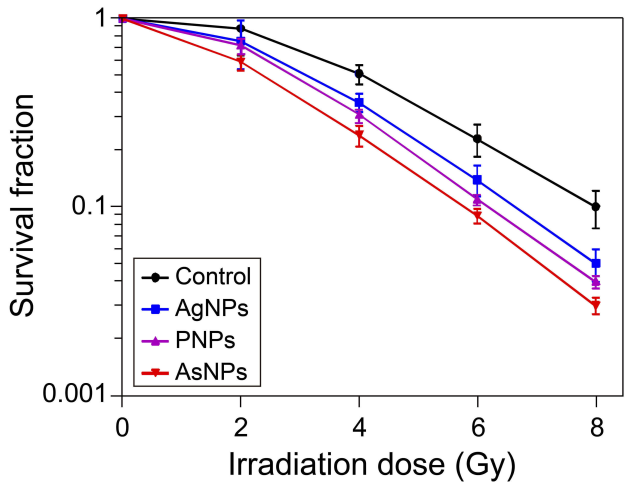

Figure 6 Effects of AgNPs, PNPs and AsNPs plus irradiation on colony formation of C6 cells.
Notes: Data are shown as the mean ± SD (n = 3).
Abbreviations: AgNPs, silver nanoparticles; PNPs, PEGylated silver nanoparticles; AsNPs, PEG- and As1411-functionalized silver nanoparticles; SD, standard deviation; n, number.

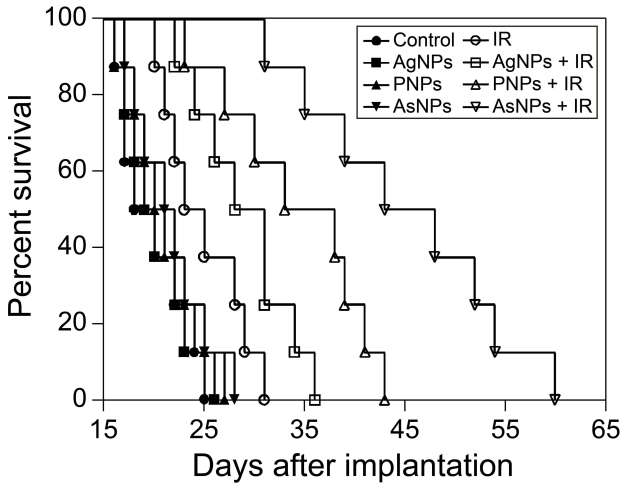

Figure 7 Kaplan-Meier survival curves for C6 glioma-bearing mice following intravenous administration of saline, AgNPs, PNPs or AsNPs with or without irradiation.
Notes: Nine days after tumor implantation, the mice were systemically administered 150 μL saline or nanomaterial solution at a dose of 10 mg/kg (eight mice per group). Six hours after injection, the mice in irradiation groups were irradiated by 6 MV X-ray beams (6 Gy per mouse). IR in the figure is an abbreviation for irradiation.
Abbreviations: AgNPs, silver nanoparticles; PNPs, PEGylated silver nanoparticles; AsNPs, PEG- and As1411-functionalized silver nanoparticles; μL, microliter; mg, milligram; kg, kilogram; MV, megavolt; Gy, gray.

irradiation, AsNPs plus irradiation and irradiation control groups. The data of our in vivo antitumor experiment confirmed our in vitro results. Furthermore, there was no evidence of systemic toxicity in these animals, as judged by body weight, behavior of the mice and histological examination of major organs (data not shown).

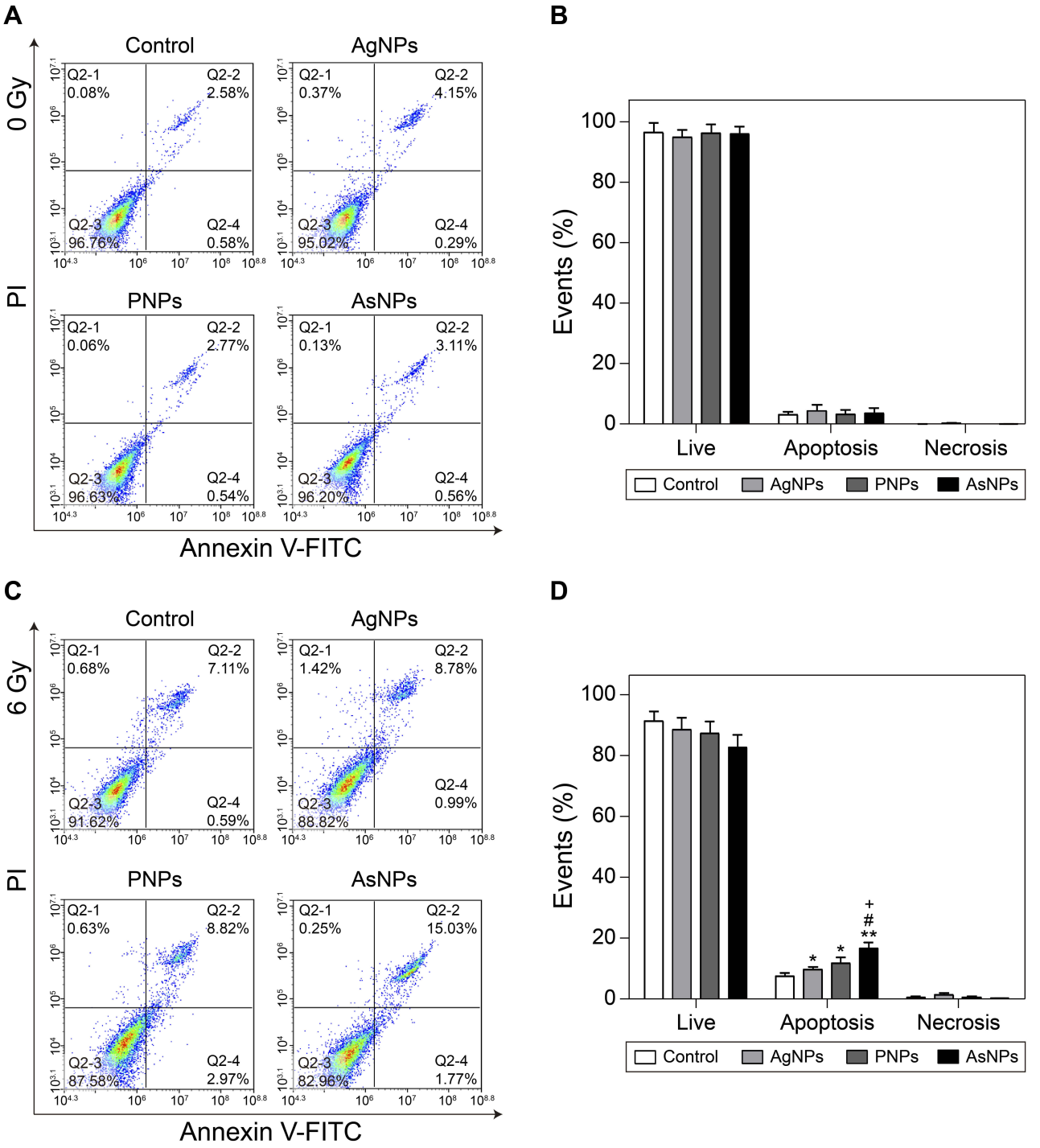

Figure 8 Apoptosis of C6 cells induced by AgNPs, PNPs or AsNPs with or without irradiation.

Notes: Representative flow cytometry images and summary of distributions of cell status without and with irradiation are shown in (**A**–**D**), respectively. Data are shown as the mean ± SD (n = 3). **P*<0.05, ***P*<0.01 compared with the irradiation control group; $^{\#}$*P*<0.05 compared with the AgNPs plus irradiation group; $^{+}$*P*<0.05 compared with the PNPs plus irradiation group.

Abbreviations: AgNPs, silver nanoparticles; PNPs, PEGylated silver nanoparticles; AsNPs, PEG- and As1411-functionalized silver nanoparticles; SD, standard deviation; n, number.

It is well known that the radiosensitizing effect of nanoparticles strongly depends on the energy of irradiating X-ray beam.[43,44] A number of experimental researches have indicated that, compared to MV radiotherapy, much higher dose enhancement values can be obtained in the case of low-energy kilovoltage radiotherapy,[45,46] which is predominantly used for superficial cancer. High-energy MV X-ray beams (10 MV and higher) are believed to be suitable to treat deep-lying tumors, owing to their superior penetration power and skin sparing.[47] However, they demonstrate lower dose enhancement compared with the 4 and 6 MV X-ray beams as predicted by Monte Carlo simulation.[48] Therefore, in the present study, we evaluated and determined the efficacy of 6 MV irradiation plus PEG- and As1411-modified AgNPs for the treatment of brain glioma.

Proapoptotic Effect of AsNPs Combined with Irradiation

Previous studies have suggested the induction of apoptosis as a potential radiosensitizing mechanism of nanosized materials.[49,50] In the current study, the apoptotic response of C6 cells to AgNPs, PNPs or AsNPs with or without 6 Gy X-ray irradiation was assessed by Annexin V-FITC/PI assay. In the non-irradiation groups, the percentages of apoptotic or necrotic cells were not strikingly different among the four groups (Figure 8A and B). When combined with irradiation, AgNPs, PNPs and AsNPs demonstrated a statistical difference in apoptotic changes as compared with irradiation control. The apoptosis rate of C6 cells induced by AsNPs plus irradiation was significantly higher than that of AgNPs or PNPs combined with irradiation. However, no significant change in the percentage of necrotic cells was observed in the radiotherapy groups (Figure 8C and D). Based on the results, it can be inferred that apoptosis, but not necrosis, was related to the cell death induced by AgNPs, PNPs or AsNPs plus irradiation, and the better radiosensitizing effect of AsNPs might be attributed to, at least in part, the higher cellular apoptosis level.

Conclusion

The aim of the present study was to construct AgNPs functionalized with PEG and As1411 (AsNPs), and evaluate their targeting property and radiosensitizing effect on glioma. It was found that AsNPs could not only be specifically uptaken by tumor cells but also effectively accumulated at the tumor site. The SER value of AsNPs was much higher than that of AgNPs and PNPs, which might be attributed to the increased apoptosis level. Furthermore, the systemic administration of AsNPs in combination with irradiation significantly prolonged the MST of C6 glioma-bearing mice. These findings have important implications for the application of AsNPs in targeted radiotherapy of brain tumors and other cancers.

Acknowledgments

This work was supported by the National Natural Science Foundation of China (81571805, 81771980 and 81703758), and the National Key Basic Research Program of China (973 Program; 2013CB933904).

Disclosure

The authors report no conflicts of interest in this work.

References

1. Brodbelt A, Greenberg D, Winters T, Williams M, Vernon S, Collins VP. Glioblastoma in England: 2007–2011. *Eur J Cancer*. 2015;51(4):533–542. doi:10.1016/j.ejca.2014.12.014
2. Louis DN, Perry A, Reifenberger G, et al. The 2016 World Health Organization classification of tumors of the central nervous system: a summary. *Acta Neuropathol*. 2016;131(6):803–820. doi:10.1007/s00401-016-1545-1
3. Pessina F, Navarria P, Cozzi L, et al. Value of surgical resection in patients with newly diagnosed grade III glioma treated in a multimodal approach: surgery, chemotherapy and radiotherapy. *Ann Surg Oncol*. 2016;23(9):3040–3046. doi:10.1245/s10434-016-5222-3
4. Shen H, Hau E, Joshi S, Dilda PJ, McDonald KL. Sensitization of glioblastoma cells to irradiation by modulating the glucose metabolism. *Mol Cancer Ther*. 2015;14(8):1794–1804. doi:10.1158/1535-7163.MCT-15-0247
5. Kwatra D, Venugopal A, Anant S. Nanoparticles in radiation therapy: a summary of various approaches to enhance radiosensitization in cancer. *Transl Cancer Res*. 2013;2(4):330–342. doi:10.3978/j.issn.2218-676X.2013.08.06
6. Kim JH, Jenrow KA, Brown SL. Mechanisms of radiation-induced normal tissue toxicity and implications for future clinical trials. *Radiat Oncol J*. 2014;32(3):103–115. doi:10.3857/roj.2014.32.3.103
7. Liu P, Huang Z, Chen Z, et al. Silver nanoparticles: a novel radiation sensitizer for glioma? *Nanoscale*. 2013;5(23):11829–11836. doi:10.1039/c3nr01351k
8. Ma N, Wu F, Zhang X, et al. Shape-dependent radiosensitization effect of gold nanostructures in cancer radiotherapy: comparison of gold nanoparticles, nanospikes, and nanorods. *ACS Appl Mater Interfaces*. 2017;9(15):13037–13048. doi:10.1021/acsami.7b01112
9. Dimitriou NM, Tsekenis G, Balanikas EC, et al. Gold nanoparticles, radiations and the immune system: current insights into the physical mechanisms and the biological interactions of this new alliance towards cancer therapy. *Pharmacol Ther*. 2017;178:1–17. doi:10.1016/j.pharmthera.2017.03.006
10. Spyratou E, Makropoulou M, Efstathopoulos EP, Georgakilas AG, Sihver L. Recent advances in cancer therapy based on dual mode gold nanoparticles. *Cancers (Basel)*. 2017;9:12. doi:10.3390/cancers9120173
11. Xu R, Ma J, Sun X, et al. Ag nanoparticles sensitize IR-induced killing of cancer cells. *Cell Res*. 2009;19(8):1031–1034. doi:10.1038/cr.2009.89
12. Ma J, Xu R, Sun J, Zhao D, Tong J, Sun X. Nanoparticle surface and nanocore properties determine the effect on radiosensitivity of cancer cells upon ionizing radiation treatment. *J Nanosci Nanotechnol*. 2013;13(2):1472–1475. doi:10.1166/jnn.2013.6087

13. Liu P, Jin H, Guo Z, et al. Silver nanoparticles outperform gold nanoparticles in radiosensitizing U251 cells in vitro and in an intracranial mouse model of glioma. *Int J Nanomedicine*. 2016;11:5003–5014. doi:10.2147/IJN.S115473
14. Leach MW, Rottman JB, Hock MB, Finco D, Rojko JL, Beyer JC. Immunogenicity/hypersensitivity of biologics. *Toxicol Pathol*. 2014;42(1):293–300. doi:10.1177/0192623313510987
15. Zhu J, Huang H, Dong S, Ge L, Zhang Y. Progress in aptamer-mediated drug delivery vehicles for cancer targeting and its implications in addressing chemotherapeutic challenges. *Theranostics*. 2014;4(9):931–944. doi:10.7150/thno.9663
16. Wu D, Gao Y, Qi Y, Chen L, Ma Y, Li Y. Peptide-based cancer therapy: opportunity and challenge. *Cancer Lett*. 2014;351(1):13–22. doi:10.1016/j.canlet.2014.05.002
17. Guo J, Gao X, Su L, et al. Aptamer-functionalized PEG-PLGA nanoparticles for enhanced anti-glioma drug delivery. *Biomaterials*. 2011;32(31):8010–8020. doi:10.1016/j.biomaterials.2011.07.004
18. Li L, Hou J, Liu X, et al. Nucleolin-targeting liposomes guided by aptamer AS1411 for the delivery of siRNA for the treatment of malignant melanomas. *Biomaterials*. 2014;35(12):3840–3850. doi:10.1016/j.biomaterials.2014.01.019
19. Huang Z, Jiang H, Liu P, et al. Continuous synthesis of size-tunable silver nanoparticles by a green electrolysis method and multi-electrode design for high yield. *J Mater Chem A*. 2015;3(5):1925–1929. doi:10.1039/C4TA06782G
20. Gao H, Qian J, Cao S, et al. Precise glioma targeting of and penetration by aptamer and peptide dual-functioned nanoparticles. *Biomaterials*. 2012;33(20):5115–5123. doi:10.1016/j.biomaterials.2012.03.058
21. Ma N, Jiang Y, Zhang X, et al. Enhanced radiosensitization of gold nanospikes via hyperthermia in combined cancer radiation and photothermal therapy. *ACS Appl Mater Interfaces*. 2016;8(42):28480–28494. doi:10.1021/acsami.6b10132
22. Murdock RC, Braydich-Stolle L, Schrand AM, Schlager JJ, Hussain SM. Characterization of nanomaterial dispersion in solution prior to in vitro exposure using dynamic light scattering technique. *Toxicol Sci*. 2008;101(2):239–253. doi:10.1093/toxsci/kfm240
23. Jokerst JV, Lobovkina T, Zare RN, Gambhir SS. Nanoparticle PEGylation for imaging and therapy. *Nanomedicine (Lond)*. 2011;6(4):715–728. doi:10.2217/nnm.11.19
24. Dubey P, Matai I, Kumar SU, Sachdev A, Bhushan B, Gopinath P. Perturbation of cellular mechanistic system by silver nanoparticle toxicity: cytotoxic, genotoxic and epigenetic potentials. *Adv Colloid Interface Sci*. 2015;221:4–21. doi:10.1016/j.cis.2015.02.007
25. Duan X, Li Y. Physicochemical characteristics of nanoparticles affect circulation, biodistribution, cellular internalization, and trafficking. *Small*. 2013;9(9–10):1521–1532. doi:10.1002/smll.201201390
26. Swanner J, Mims J, Carroll DL, et al. Differential cytotoxic and radiosensitizing effects of silver nanoparticles on triple-negative breast cancer and non-triple-negative breast cells. *Int J Nanomedicine*. 2015;10:3937–3953. doi:10.2147/IJN.S80349
27. Ba H, Rodriguez-Fernandez J, Stefani FD, Feldmann J. Immobilization of gold nanoparticles on living cell membranes upon controlled lipid binding. *Nano Lett*. 2010;10(8):3006–3012. doi:10.1021/nl101454a
28. Antosh MP, Wijesinghe DD, Shrestha S, et al. Enhancement of radiation effect on cancer cells by gold-pHLIP. *Proc Natl Acad Sci U S A*. 2015;112(17):5372–5376. doi:10.1073/pnas.1501628112
29. Li H, Du J, Du X, et al. Stimuli-responsive clustered nanoparticles for improved tumor penetration and therapeutic efficacy. *Proc Natl Acad Sci U S A*. 2016;113(15):4164–4169. doi:10.1073/pnas.1522080113
30. Lai Y, Chiang C, Kao T, Chen S. Dual-drug nanomedicine with hydrophilic F127-modified magnetic nanocarriers assembled in amphiphilic gelatin for enhanced penetration and drug delivery in deep tumor tissue. *Int J Nanomedicine*. 2018;13:3011–3026. doi:10.2147/IJN.S161314
31. Ren Y, Mu Y, Song Y, et al. A new peptide ligand for colon cancer targeted delivery of micelles. *Drug Deliv*. 2016;23(5):1763–1772. doi:10.3109/10717544.2015.1077293
32. Wu J, Song C, Jiang C, Shen X, Qiao Q, Hu Y. Nucleolin targeting AS1411 modified protein nanoparticle for antitumor drugs delivery. *Mol Pharm*. 2013;10(10):3555–3563. doi:10.1021/mp300686g
33. Cao C, Zhang J, Wen X, et al. Metamaterials-based label-free nanosensor for conformation and affinity biosensing. *ACS Nano*. 2013;7(9):7583–7591. doi:10.1021/nn401645t
34. Hovanessian AG, Soundaramourty C, El KD, Nondier I, Svab J, Krust B. Surface expressed nucleolin is constantly induced in tumor cells to mediate calcium-dependent ligand internalization. *PLoS One*. 2010;5(12):e15787. doi:10.1371/journal.pone.0015787
35. Goswami N, Luo Z, Yuan X, Leong DT, Xie J. Engineering gold-based radiosensitizers for cancer radiotherapy. *Mater Horiz*. 2017;4(5):817–831. doi:10.1039/c7mh00451f
36. Hadjidemetriou M, Al-Ahmady Z, Kostarelos K. Time-evolution of in vivo protein corona onto blood-circulating PEGylated liposomal doxorubicin (DOXIL) nanoparticles. *Nanoscale*. 2016;8(13):6948–6957. doi:10.1039/c5nr09158f
37. Chiu C, Chung T, Chen S, Ma Y. Effects of PEGylation on capture of dextran-coated magnetic nanoparticles in microcirculation. *Int J Nanomedicine*. 2019;14:4767–4780. doi:10.2147/IJN.S204844
38. Muhamad N, Plengsuriyakarn T, Na-Bangchang K. Application of active targeting nanoparticle delivery system for chemotherapeutic drugs and traditional/herbal medicines in cancer therapy: a systematic review. *Int J Nanomedicine*. 2018;13:3921–3935. doi:10.2147/IJN.S165210
39. Li R, Zheng K, Yuan C, Chen Z, Huang M. Be active or not: the relative contribution of active and passive tumor targeting of nanomaterials. *Nanotheranostics*. 2017;1(4):346–357. doi:10.7150/ntno.19380
40. Gerweck LE, Wakimoto H. At the crossroads of cancer stem cells, radiation biology, and radiation oncology. *Cancer Res*. 2016;76(5):994–998. doi:10.1158/0008-5472.CAN-15-2455
41. Su X, Liu P, Wu H, Gu N. Enhancement of radiosensitization by metal-based nanoparticles in cancer radiation therapy. *Cancer Biol Med*. 2014;11(2):86–91. doi:10.7497/j.issn.2095-3941.2014.02.003
42. Coulter JA, Jain S, Butterworth KT, et al. Cell type-dependent uptake, localization, and cytotoxicity of 1.9 nm gold nanoparticles. *Int J Nanomedicine*. 2012;7:2673–2685. doi:10.2147/IJN.S31751
43. Taupin F, Flaender M, Delorme R, et al. Gadolinium nanoparticles and contrast agent as radiation sensitizers. *Phys Med Biol*. 2015;60(11):4449–4464. doi:10.1088/0031-9155/60/11/4449
44. Lin Y, McMahon SJ, Scarpelli M, Paganetti H, Schuemann J. Comparing gold nano-particle enhanced radiotherapy with protons, megavoltage photons and kilovoltage photons: a Monte Carlo simulation. *Phys Med Biol*. 2014;59(24):7675–7689. doi:10.1088/0031-9155/59/24/7675
45. Youkhana EQ, Feltis B, Blencowe A, Geso M. Titanium dioxide nanoparticles as radiosensitisers: an in vitro and phantom-based study. *Int J Med Sci*. 2017;14(6):602–614. doi:10.7150/ijms.19058
46. Kong T, Zeng J, Wang X, et al. Enhancement of radiation cytotoxicity in breast-cancer cells by localized attachment of gold nanoparticles. *Small*. 2008;4(9):1537–1543. doi:10.1002/smll.200700794
47. Zhang Y, Feng Y, Ming X, Deng J. Energy modulated photon radiotherapy: a Monte Carlo feasibility study. *Biomed Res Int*. 2016;2016:7319843. doi:10.1155/2016/7319843
48. Hwang C, Kim JM, Kim J. Influence of concentration, nanoparticle size, beam energy, and material on dose enhancement in radiation therapy. *J Radiat Res*. 2017;58(4):405–411. doi:10.1093/jrr/rrx009
49. Chang M, Shiau A, Chen Y, Chang C, Chen H, Wu C. Increased apoptotic potential and dose-enhancing effect of gold nanoparticles in combination with single-dose clinical electron beams on tumor-bearing mice. *Cancer Sci*. 2008;99(7):1479–1484. doi:10.1111/j.1349-7006.2008.00827.x
50. Teraoka S, Kakei Y, Akashi M, et al. Gold nanoparticles enhance X-ray irradiation-induced apoptosis in head and neck squamous cell carcinoma in vitro. *Biomed Rep*. 2018;9(5):415–420. doi:10.3892/br.2018.1142